International Journal of Thermal Sciences 48 (2009) 1247–1258

Contents lists available at ScienceDirect

International Journal of Thermal Sciences

www.elsevier.com/locate/ijts

Analysis of conduction – natural convection conjugate heat transfer in the gap between concentric cylinders under solar irradiation

Dong Chul Kim, Young Don Choi *

Department of Mechanical Engineering, Korea University, Anam-dong, Sungbuk-ku, Seoul 136-701, South Korea

ARTICLE INFO

Article history:
Received 29 January 2008
Received in revised form 7 October 2008
Accepted 4 November 2008
Available online 6 December 2008

Keywords:
Inner cylinder (gun)
Outer cylinder (shield tube)
Solar radiation
Natural convection

ABSTRACT

Although, in general, most of concentric cylinders used in engineering applications are heated non-uniformly, studies on the natural convection in the air layer between the cylinders have been performed only for the uniform heating so that it is difficult to apply the results to the real cases. In the present study, the effects of material property of outer cylinder and the air gap thickness between cylinders on the natural convection are investigated by computational fluid dynamics and experimental means. Namely, conduction-natural convection conjugated heat transfer in the concentric cylinders, gun and shield tube, under solar irradiation, is analyzed numerically and the various predictions on the resultant thermal deformations of gun are compared to the experimental data with variation of the gap thickness of cylinders and material properties of shield tube. Results show that larger the thermal conductivity of shield tube, smaller the Nusselt number variations of gun and shield tube surfaces. This is due to that balance of conduction in the cylinders and natural convection in the gap between inner and outer cylinders may increase the uniformity of the air layer temperature. High thermal conductivity of shield tube inhibits the natural convection in the air layer and there exists a gap thickness that exerts an influence critically on the thermal deformation of gun.

1. Introduction

Studies on the natural convection of the air gap in a double cylinder assume that a uniform heat is transferred to the inner or outer cylinder and cause the temperature difference between the cylinders to generate natural convection. Most cylinders used in engineering applications are, however, heated nonuniformly, and, there has been little research on natural convection caused by nonuniform heating. A typical example of cylinders showing nonuniform heating is the gun of a tank, which is heated by solar radiation energy. The accuracy of the first shot of a tank gun is an important factor that can decide the direction of a battle. Sunlight and wind, etc. are the environmental conditions that influence the accuracy of the first shot of a tank gun exposed to outside environment. Among these conditions, solar radiation is the most influential factor that can lower the shot accuracy because it generates temperature nonuniformity in the gun and consequently, the deformation of the gun. Tank guns are usually shielded by a tube in the axial direction to protect them from environmental conditions. The cylindrical tube, called the shield tube, shields the gun and distributes uniform temperature around it minimizing the deformation of the gun. In the tank exposed to direct solar radiation, various types of secondary flow patterns occur in the air layer between the gun and shield tube, according to the gap thickness between the gun and shield tube, and the material of the shield tube. These secondary flow patterns may affect the gun temperature. It is important to understand the characteristics of the secondary flow in the air layer between the shield tube and gun in the analysis of the phenomena that influence the gun temperature. Many studies have been performed on the natural convection in the gap between two horizontal cylinders to apply the results to various industrial designs such as the solar heat collector, cooling system of a nuclear reactor, regenerator and heat exchanger. Concerning the natural convection problem in a closed space of two horizontal cylinders, Beckmann [1] first began to study the secondary flow characteristics with respect to the inner-to-outer diameter ratio of the cylinders. Then, in the 1960's, Eckert [2] experimentally investigated natural convection heat transfer in a closed space by using the Mach–Zehnder interferometer, and many papers since then have been published on this method [3,4]. Grigull and Hauf [5] made a classification based on their experiments with an interferometer, into the two-dimensional pseudo-conductive area, the three-dimensional transition area and the developed secondary laminar flow natural convection area. Crawford et al. [6] numerically analyzed the phenomenon of natural convection in horizontal cylinder space and obtained the streamlines of crescent and kidney

* Corresponding author. Tel.: +82 2 3290 3355; fax: +82 2 928 1067.
E-mail address: ydchoi@korea.ac.kr (Y.D. Choi).

1290-0729/$ – see front matter
doi:10.1016/j.ijthermalsci.2008.11.005

Nomenclature

A	area of air layer
C_p	specific heat
D^*_{point}	comprehensively express the air gap thickness between the gun and shield tube
D^*_1	gun that not shrouded by a shield tube
D_1	diameter of inner wall in shield tube
d_2	diameter of outer wall in gun
E	modulus of elasticity
h_θ	local heat transfer coefficient
$\overline{h_\theta}$	average heat transfer coefficient
I	secondary flow intensity
I	radiation intensity
I_b	radiation intensity of black body
I_D	direct solar radiation
I_d	diffuse solar radiation
I_{total}	solar radiation intensity
I_r	reflected solar radiation
L	annular gap $(= (R_1 - r_2))$
M_{point}	material changes of the shield tubes
n	number of grid points
Nu_θ	local Nusselt number
$\overline{Nu_\theta}$	average values of Nusselt number
Pr	Prandtl number
q_r	radiation heat flux
q_{R_2}	heat flux between outer surface of shield tube and ambient air
q_{solar}	solar radiation heat flux on the tilted shield tube position
q_θ	local heat flux at θ degree
Ra_L	Rayleigh number
$\overline{T_{s1}}$	average temperature of shield tube at D_1 point
$\overline{T_{g2}}$	average temperature of gun at d_2 point
T_k	grid point temperature
$T_{s\theta}$	local surface temperature
$T_{b\theta}$	local bulk air temperature
T_{br}	local bulk temperature at r distance
$\overline{T}_\infty$	ambient temperature
u	velocity in radial direction
$\bar{u}$	displacements in the z directions
v	velocity in angular direction
$\bar{v}$	displacements in the θ directions
$\bar{w}$	displacements in the r directions

Greek symbols

α	thermal diffusivity
α_A	sky clearness coefficient
β	thermal expansion coefficient
γ	shear strain
ε	normal strain
ε'	emissivity
θ	angle (degree)
k	thermal conductivity
μ	dynamic viscosity
ν	kinematic viscosity
$\nu_{\text{Poisson's ratio}}$	Poisson's ratio
ξ, η	direction of solid angle $(\vec{\Omega})$
ρ	fluid density
ρ_r	reflexibility
σ	normal stresses
σ_g	standard deviation of gun temperature
σ_s	Stefan–Boltzmann constant
τ	shear stresses
χ	absorption coefficient
$\vec{\Omega}$	solid angle

shaped vortex flow. Grigull and Hauf [7] catalogued the natural convection flow into the similarity conduction region, the transition region, and the fully developed, two-dimensional, laminar flow region, by visualization experiments using smoke. Mack and Bishop [8] found that, in a cylinder of diameter-to-length ratio $D/L = 2$, the steady state natural convection of fluid of $Pr = 0.02$ generates two eddies. Through this experiment, they elucidated the occurrence of multi-cell flow for $Ra = 300$ in liquid metal of a low Prandtl number. Kuehn and Goldstein [9] used the Mach–Zehnder interferometer to measure local heat transfer coefficients and temperature distributions in a cylinder space of gap thickness-to-diameter ratio of 0.8 and in the range of Rayleigh numbers between 2.11×10^4–9.76×10^6. They also numerically investigated the effects of the Prandtl number and ratio of diameters by using the finite difference method. Moreover, they extended their research to examine the same effects according to the eccentricity ratio in non-concentric annular cylinder space. Rao et al. [10] determined numerically and experimentally that a unit cell vortex can break down into a multicellular pattern in the horizontal cylinder by the increase in the Rayleigh number. At a given Nusselt number and diameter ratio, they compared the dominant flow patterns and the temperature distributions. Castrejon and Spalding [11] also performed similar studies for the conditions, $Pr = 7.0$, $Ra = 6.3 \times 10^8$ and $D_2/D_1 = 15.9$. From the results, continuous pictures of the thermal flame of the heated fluid were obtained. The experimental and theoretical results showed the consistency in the physical properties. In regard to the natural convection heat transfer in a cylinder, Hamad and Khan [12] determined that the diameter ratio and the Rayleigh number affect the flow characteristics more dominantly than the inclination angle of the cylinder axis. Yoo [13–16] investigated systematically the convection and bifurcation phenomena. Thermal and hydrodynamic instabilities in an annular cylinder generate various forms of secondary flow patterns and transition phenomenon according to the Prandtl number. Horng Wen Wu et al. [17] studied the transient natural convection for a fluid with a high Prandtl number in a sphere with a vertical eccentricity. An unsteady natural convection in a horizontal annulus was investigated by Mizushima et al. [18]. Shahraki [19] demonstrated the effect of temperature-dependent properties on the streamlines and temperature distributions in a concentric annulus. Petrone et al. [20] numerically studied the linear instability of two-dimensional natural convection in air-filled horizontal annuli, and a map of possible flow patterns was established. N.A. Roschina et al. [21] studied the natural convection in an annulus between coaxial horizontal cylinders with internal heat generation. Abdalla M. Al-Amiri et al. [22] studied the numerical simulation of double-diffusive mixed convection within a rotating horizontal annulus. J.C. Leong et al. [23] studied the natural convection in a concentric annulus with a porous sleeve. Takahiro Adachi et al. [24] studied the three-dimensional linear stability natural convection in horizontal concentric annuli. Khalil Khanafer et al. [25] studied the Numerical analysis of natural convection heat transfer in a horizontal annulus partially filled with a fluid-saturated porous substrate.

As mentioned, the many studies on the natural convection occurring between two cylinders have been about the natural convection arising from the temperature difference between the inner and outer walls of a cylinder that is heated uniformly. This study

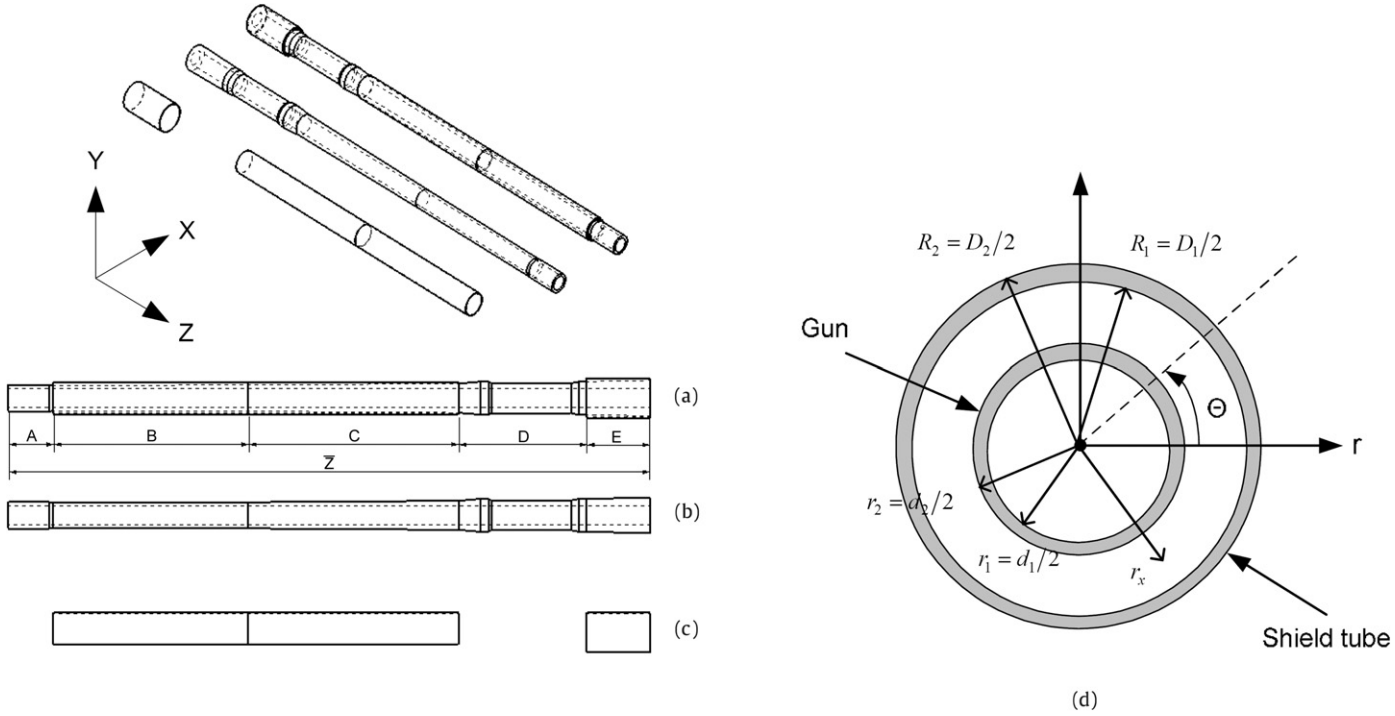

Fig. 1. Schematic of gun and shield tube.

Table 1
Material properties of gun and shield tube.

Properties	ρ (Kg/m^3)	k (W/m K)	C_p (J/Kg K)	$\alpha = (\frac{k}{\rho C_p})$ (10^{-7} m^2/s)	E (GN/m^2)	νPoisson's ratio
Shield tube						
Gun	7850	44.5	475	11.93	203.98	0.28
FRP	2540	1.0344	795.5	5.12	Not available	
Titanium	4850	7.44	544.25	28.19		
Steel	8030	16.27	502.48	40.32		
Nickel	8900	91.74	460.6	223.79		
Aluminum	2719	202.4	871	854.64		
Gold	19320	297.73	129.81	1187.15		
Copper	8978	387.6	381	1133.13		

is, thus, to handle a gun (an inner cylinder) and a shield tube (an outer cylinder), which are thought to be a typical double cylinder nonuniformly heated by the solar radiation energy, and to carry out experiments on the thermal diffusion and flow circulation by considering the materials of the shield tube, as an outer cylinder, and the thickness of the air layer between the cylinders, for the purpose of finding out their effects on the natural convection between the cylinders.

2. Mathematical analysis

2.1. Analysis method

Fig. 1 illustrates the shapes of the gun (inner cylinder) and shield tube (outer cylinder), where (b) is the gun, (c) is the shield tube, and (a) is the assembly of both. The shield tube enclosing the gun is composed of three parts, and the gap between the gun and shield tube forms the air layer. The shield tube comprises about 73% of the gun assembly. (d) illustrates the cross-sections of the gun and shield tube for the shield tube to gun diameter ratio of the shield tube of $D_1/d_2 = 1.149$.

Table 1 shows the material properties of the gun and shield tube examined in the present study.

In general, it is the unsteadiness of the fluid flow in the cylinder gap that makes the heat transfer complex. In the gap between the gun and shield tube, the Rayleigh number is defined as

$$Ra_L = \frac{g\beta(\overline{T}_{s1} - \overline{T}_{g2})L^3}{\nu^2}Pr \tag{1}$$

The temperature difference between the outer surface of the gun and the inner surface of the shield tube is the main cause of the natural convection in the gap. The Rayleigh number defined as Eq. (1) is in the range of $0.0063 \leqslant Ra_L \leqslant 7.5 \times 10^4$. Therefore, the natural convection is laminar flow. The deviation of gun temperature induces the thermal deformation of the gun. As the thermal deviation increases, the deformation increases accordingly. The standard deviation (σ_g) of gun temperature can be used to indicate the effects of temperature nonuniformity in the gun. Standard deviation is defined as.

$$\sigma_g = \sqrt{\left(\sum_{k=1}^{n}(T_k - \overline{T_g})^2\right)\Big/ n} \tag{2}$$

where T_k: grid point temperature; n: number of grid points.

Secondary flow intensity described by Eq. (3) is also used to explain the characteristics of natural convection.

$$I = \frac{\int(\sqrt{u^2 + v^2})\,dA}{A} \tag{3}$$

where A: area of air layer; u: velocity in radial direction; v: velocity in angular direction.

In Table 2, D^*_{point} is introduced to comprehensively express the air gap width between the gun and shield tube. D^*_1 represents the case in which the gun is not shrouded by a shield tube, and thus is exposed to direct solar radiation. M_{point} represents the material changes of the shield tubes.

Table 2
Definitions of D^* , and M.

Point	$D^*_{\text{point}} = (D_1/d_2)$	M_{point}
1	1	FRP
2	1.006	Titanium
3	1.018	Steel
4	1.030	Nickel
5	1.042	Aluminum
6	1.060	Gold
7	1.077	Copper
8	1.089	Not available
9	1.119	
10	1.149	
11	1.268	
12	1.367	
13	1.506	
14	1.625	
15	1.744	

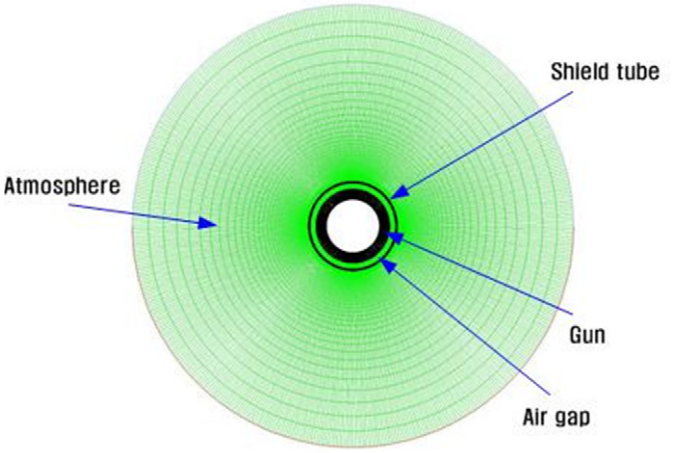

(a)

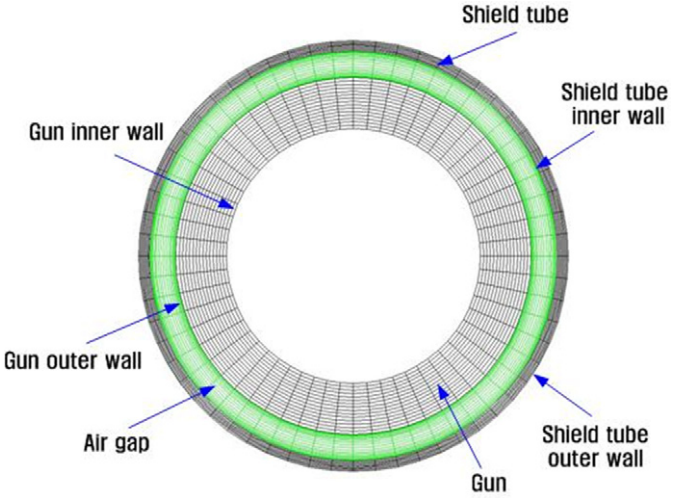

(b)

Fig. 2. Grid generations (2D).

2.2. Numerical method

2.2.1. Thermal flow analysis

The shapes of the air layer in the gap between the gun and shield tube are assumed unchanging in the axial direction. Therefore, the calculation domain is two-dimensional.

Fig. 2(a) shows the grid generation of the outside region of the shield tube. This grid is used to calculate the natural convection heat transfer around the shield tube. The standard grid of the outside region of shield tube was 158×528 in the radial and circumferential directions, respectively. The size of the outside computation domain in the radial direction was about 40 times the air gap width between the gun and shield tube. Gambit V2.0 program was used for grid generation. Fig. 2(b) shows the grid generation for the shield tube, air layer and gun.

The standard grids employed to cover the half cross-sections of the shield tube, air layer and gun were 6×528, 48×528, and 24×528, respectively. Uniform grids were generated for the gun and shield tube, but nonuniform grids were employed for the air layer, a dense grid near the walls and a sparse grid in the core region. The study tested grid number dependence on the results. Grid numbers are increased until the results reach the grid independent state. All simulations are performed at this grid independent grid number condition.

Fluent V6.1 [25] was employed to solve the momentum and energy equations for the natural convection in the gap between the gun and shield tube. Staggered grid and SIMPLE algorithm were adopted. A segregated solver was used to calculate the velocity components. The governing equations for momentum and energy were the simultaneous partial differential equations obtained by applying the conservations of momentum and energy to the local control volume. Boussinesq approximation was used to model the buoyancy terms in the governing equations, because the temperature difference in the air layer was not large. In the Boussinesq approximation, the density variation due to temperature change was assumed to affect the buoyancy terms.

The governing equations for momentum and energy around the cross-section of the air layer are conveniently expressed in cylindrical coordinates.

The governing equations in cylindrical coordinate, including Boussinesq buoyancy term, for 2D laminar natural convection are given by:

- Continuity equation

$$\frac{1}{r}\frac{\partial(ru)}{\partial r} + \frac{1}{r}\frac{\partial v}{\partial \theta} = 0 \tag{4}$$

- Momentum equation in the radial direction

$$\frac{\partial u}{\partial t} + u\frac{\partial u}{\partial r} + \frac{v}{r}\frac{\partial u}{\partial \theta} - \frac{v^2}{r} = \frac{1}{\rho}\left[\rho g\beta(T - T_\infty)\sin(\theta) - \frac{\partial p}{\partial r}\right] + \nu\left[\frac{\partial^2 u}{\partial r^2} + \frac{1}{r}\frac{\partial u}{\partial r} - \frac{u}{r^2} + \frac{1}{r^2}\frac{\partial^2 u}{\partial \theta^2} - \frac{2}{r^2}\frac{\partial v}{\partial \theta}\right] \tag{5}$$

- Momentum equation in the circumferential direction

$$\frac{\partial v}{\partial t} + u\frac{\partial v}{\partial r} + \frac{v}{r}\frac{\partial v}{\partial \theta} + \frac{uv}{r} = \frac{1}{\rho}\left[\rho g\beta(T - T_\infty)\cos(\theta) - \frac{1}{r}\frac{\partial p}{\partial \theta}\right] + \nu\left[\frac{\partial^2 v}{\partial r^2} + \frac{1}{r}\frac{\partial v}{\partial r} - \frac{v}{r^2} + \frac{1}{r^2}\frac{\partial^2 v}{\partial \theta^2} + \frac{2}{r^2}\frac{\partial u}{\partial \theta}\right] \tag{6}$$

- Energy equation

$$\frac{\partial T}{\partial t} + u\frac{\partial T}{\partial r} + \frac{v}{r}\frac{\partial T}{\partial \theta} = \alpha\nabla^2 T \tag{7}$$

where $\nabla^2 \equiv [\frac{\partial^2}{\partial r^2} + \frac{1}{r}\frac{\partial}{\partial r} + \frac{1}{r^2}\frac{\partial^2}{\partial \theta^2}]$.

The corresponding boundary conditions are given below

Inner surface of inner cylinder (gun)

$$r = r_1: \quad \frac{\partial T}{\partial r} = 0$$

Outer surface of inner cylinder (gun)

$$r = r_2: \quad u = 0, \qquad v = 0$$

Inner surface of outer cylinder (shield tube)

$$r = R_1: \quad u = 0, \qquad v = 0$$

Outer surface of outer cylinder (shield tube)

$r = R_2$:

(1) $q_{\text{solar}} = I_{\text{total}}$ (W/m^2) Solar radiation heat flux on the tilted shield tube position.
(2) $q_{R_2} = h(\overline{T}_{s1} - \overline{T}_\infty) + \varepsilon'\sigma_s(\overline{T}_{s1}^4 - \overline{T}_\infty^4)$ Heat transfer between outer surface of shield tube and ambient air, where
$u, v =$ Velocity components in cylindrical coordinate system.
$\sigma_s =$ Stefan–Boltzmann constant.
$\overline{T}_\infty =$ Ambient temperature.

With initial condition, the temperature of inner and the outer wall of inner cylinder considered at ambient temperature. The heat transfer by solar radiant energy is transferred in the inner cylinder through outer cylinder and air layer gap. So the natural convection occurs because of the temperature difference of the outer wall of inner cylinder and the inner wall of external cylinder.

Air is transmittable medium of thermal radiation, but the shield tube and gun are not transmittable. The emissivities of all the walls were assumed to be constant. The radiation heat flux q_r in the energy equation (7) can be obtained by solving the radiative transfer equation (RTE).

To calculate the wall temperature, the local energy equilibrium described as Eq. (8) is employed.

$$(-k\nabla T + \vec{q}_r)\cdot\vec{n} = 0 \tag{8}$$

In the case of mixed convection with radiation, the radiation heat flux (q_r) appearing in Eq. (8) should be determined. In the case of surface radiation without consideration of scattering, the radiation heat flux terms can be obtained by solving the radiation transfer equation. Usually, for an absorbing and emitting medium, the radiation transfer equation is described by Eq. (9).

$$\xi\frac{\partial I}{\partial x} + \eta\frac{\partial I}{\partial y} = -\chi I + \chi I_b \tag{9}$$

In the present study, the Discrete Ordinate Method (DOM) [25] was employed to solve the radiation transfer equation. The boundary condition for the radiation transfer equation is as follows.

$$I(x, y, \vec{\Omega}) = \varepsilon' I_b(x, y) + \frac{\rho_r}{\pi}\int_{n\cdot\Omega'<0} |\vec{n}\cdot\vec{\Omega}|I(x, y, \vec{\Omega}')\,d\Omega' \tag{10}$$

Here, $I(x, y, \vec{\Omega})$ is the radiation intensity leaving the wall, ε' is emissivity, ρ_r is reflexibility, and $\vec{n}$ is the unit outward normal vector to the wall. The right side of Eq. (10) represents the radiation and reflection energies to the wall. If the radiation intensity is calculated by combining Eq. (9) and the boundary condition (10), radiant heat flux (q_r) in Eq. (8) can be obtained by the following equation.

$$\vec{q}_r = \int_{4\pi} I(x, y, \vec{\Omega})\,d\vec{\Omega} \tag{11}$$

Table 3
Calculation conditions.

Items	Conditions
Location	North latitude: 38°9′ East longitude: 127°19′
Date standard	September 21
Solar hour (o'clock)	8, 9, 10, 11, 12, 13, 14, 15, 16

2.2.2. Solar radiation energy

Solar radiation intensity should be considered precisely in the calculation of radiation heat flux. The total short-wavelength irradiance I_{total} reaching terrestrial surface is the sum of the direct solar radiation I_D, the diffuse sky radiation I_d, and the solar radiation I_r reflected from surrounding surfaces. The irradiance on the terrestrial surface of the beam component I_D is the product of the direct normal irradiation I_{DN} and the cosine of the angle of incidence θ between the incoming solar rays and a line normal to the surface:

$$I_{\text{total}} = I_{DN}\cos\theta_i + I_d + I_r \tag{12}$$

The equations are presented in ASHRAE Handbook of Fundamentals [26]. As for equation values presented in ASHRAE Handbook are used just as they are. But the sky clearness coefficient α_A of the day is multiplied to the value of A given in ASHRAE Handbook.

The tank examined in the present study is assumed to be located at north latitude 38°9′ and east longitude 127°19′ in South Korea, as described in Table 3.

From 8 o'clock to 16 o'clock on September 21, the solar irradiation at every hour calculated from the above equations was assumed to apply on the outer wall of the shield tube.

2.2.3. Thermal stress analysis

ANSYS V10.0 [27] was used to calculate the thermal stresses generated in the gun by solar radiation and the effect of the shield tube on the thermal deformation of the gun.

The gun temperature at every nodal point obtained by 3D calculation was required to calculate the gun deformation by structural analysis. Therefore, we generated a 3D grid system of the gun, which was composed of 31,512 nodes and 26,000 hexahedral grids, by using Gambit. In the ANSYS analysis, for the one end of the gun, the structurally fixed boundary condition was assumed, and for the other end, free condition was assumed. The real shield tube and gun have open ends so that simulations are conducted for open ends condition. Only, one end side is that fixed condition (clamp condition) applied in all displacement area, in order to embody a fixed form like tank gun actually.

The analysis is applicable to the loads which result in small deformations and linearly elastic material behavior. As described in the program statement, all the loads, and hence all resulting strains and stresses are independent of the axial coordinate z. Then, the equations of force equilibrium are

- Equilibrium equation

$$\begin{aligned} &-\frac{\partial\tau_{zr}}{\partial r} - \frac{\tau_{zr}}{r} - \frac{\partial\tau_{z\theta}}{r\partial\theta} = 0\\ &-\frac{\partial\sigma_\theta}{r\partial\theta} - \frac{\partial\tau_{\theta r}}{\partial r} - 2\frac{\tau_{\theta r}}{r} = 0\\ &\frac{\sigma_\theta}{r} - \frac{\partial\sigma_r}{\partial r} - 2\frac{\tau_{\theta r}}{r} = 0 \end{aligned} \tag{13}$$

where, as usual, σ and τ represent normal and shear stresses. The strain displacement relations are

$$\varepsilon_z = \frac{\partial\bar{u}}{\partial z}, \qquad \varepsilon_r = \frac{\partial\bar{w}}{\partial r}, \qquad \varepsilon_\theta = \frac{w}{r} + \frac{1}{r}\frac{\partial\bar{v}}{\partial\theta} \tag{14}$$

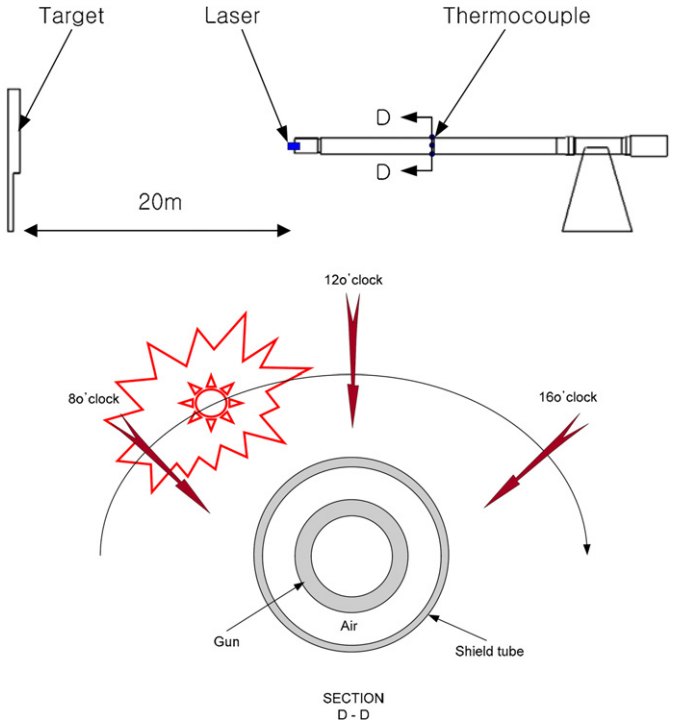

Fig. 3. Schematic showing the measurement system of gun deformation.

$$\gamma_{\theta r} = \frac{\partial \bar{w}}{r\partial\theta} + \frac{\partial \bar{v}}{\partial r} - \frac{\bar{v}}{r}$$
$$\gamma_{zr} = \frac{\partial \bar{u}}{\partial r} + \frac{\partial \bar{w}}{\partial z}$$
$$\gamma_{z\theta} = \frac{\partial \bar{u}}{r\partial\theta} + \frac{\partial \bar{v}}{\partial \bar{z}} \qquad (15)$$

where ε is the normal strain and γ is the engineering shear strain. $\bar{u}$, $\bar{v}$ and $\bar{w}$ are the displacements in the z, θ, and r directions.

2.3. Experimental setup and test procedure

Tests were performed to examine the effect of the shield tube on the gun deformation (Fig. 3). A laser source was installed at the center of the fore-end of the gun and the target was located 20 m apart from the gun. A wind blocking wall was installed around the experimental apparatus to exclude wind effects. Also, all other outside factors that could influence the accuracy of the experiments were removed, and the experiments were performed on a clear-sky day. The datum point of the laser beam at the target was taken at night when there was no gun deformation. From 8 to 16 o'clock, the deviation of the target point of the laser beam was indicated at every hour. Also, the temperature distribution of the outer wall of the gun was measured at every hour by the thermocouples installed at locations of 0°, 90°, 180°, and 270° in the cylindrical direction. The model L705 laser, manufactured by the HAMER LASER Company, was used. The rectilinearity error of the beam was 0.0025 mm per 3 m.

3. Results and discussions

3.1. Confidence test of numerical analysis

Figs. 4 and 5 show the comparison of the predicted and experimental locations of gun deformation for air gap width of D^*_{10}. The natural convections in the air gap were solved for the steady and unsteady conditions. In the steady state analysis, equilibrium between the gun and air layer temperatures was assumed at every

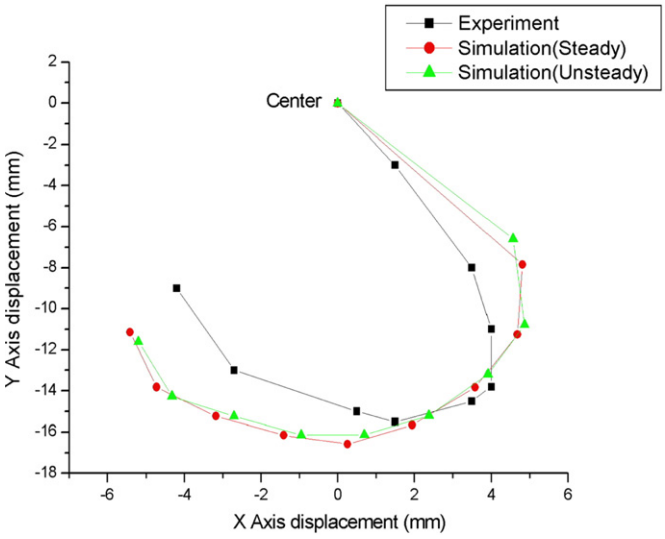

Fig. 4. Comparison of the loci of gun deformation obtained from experimental and numerical analyses.

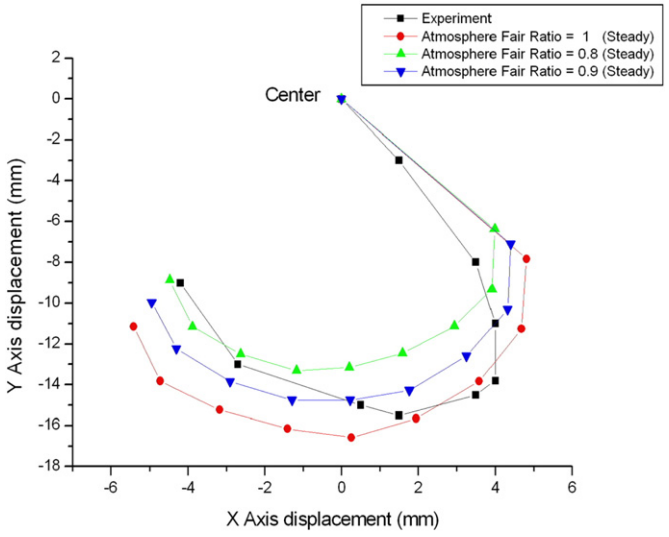

Fig. 5. Comparison of experimental and numerical gun deformations.

computation time. But, in the unsteady state analysis, the gun and air layer temperatures did not reach equilibrium instantaneously, but rather, formed continuously developing temperature fields. In the experimental analysis, the measured deformation was much greater than the actual gun deformation, because the target was located 20 m away from the gun end. According to the results of the numerical analysis, the deformation of the gun obtained from the thermal stress analysis was extended to 20 m ahead by using the Unigraphics 3D CAD equipment to magnify equally the experimental and calculated deformations of the gun. The configuration of the gun deformation forms the curve from the coordinate datum point to the other center of the gun end. The tangent to the centerline curve of the gun at the free end is extended to the target plane 20 m away from the datum plane of the gun. Then, the experimental and analytical results for the gun deformations were compared.

In Fig. 4, the gun deformations obtained by steady and unsteady numerical analyses are also compared with the experimental results. Steady and unsteady simulations gave nearly the same locus of gun deformations. Both the loci of gun deformations showed a similarity with the experimental ones. But, quantitatively, the

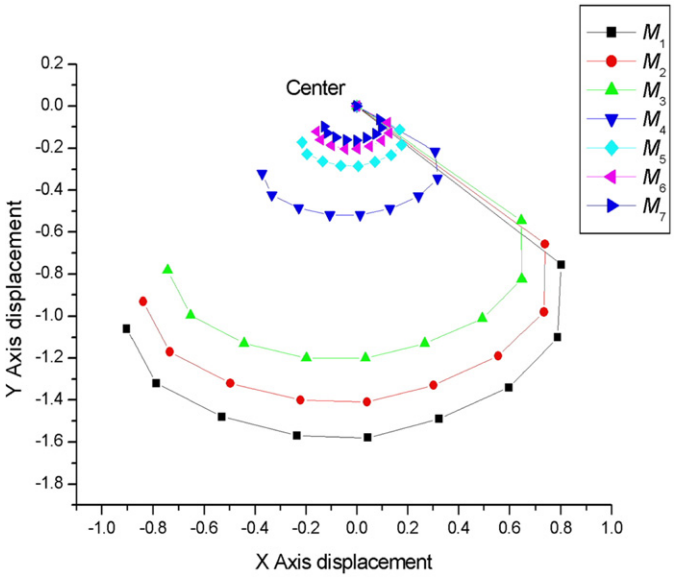

Fig. 6. Gun deformation according to material changes of shield tube.

analytical and experimental gun deformations showed considerable difference throughout the entire experimentation period. One cause of the analytical errors was the neglect of sky clearness on the day of the experiment. The weather on the day of the experiment was clear, but the clearness of the day may not have been the same as the standard value presented in the ASHRAE handbook, so the direct solar radiation on the day of the experiment would have been different from the values presented in the handbook. Another cause of the analytical error is the neglect of the wind effect based on wind speed measurements. If wind blows, the heat transfer coefficient of the outer surface of the shield tube would increase, and thereby decrease the nonconformity of the outer surface temperature of the shield tube. On the whole, the gun deformations obtained by analysis were larger than those obtained by experiments. Therefore, the possibility of the wind effect cannot be excluded. If sky clearness is low, direct solar radiation decreases, so the deformation of the gun can be decreased.

Fig. 5 shows the variation of gun deformation with respect to the sky clearness coefficient (α_A). A sky clearness coefficient of 1 means a perfectly clear day. CFD analyses were performed for two clearness coefficients $\alpha_A = 0.8$ and 0.9. The calculation results for α_A of 0.9 agreed best with the experimental results. Since the sky clearness and wind speed vary in a day, to correctly consider the sky clearness and wind effect, the experimental data on sky clearness should be used in the numerical analysis.

3.2. The effects of the changes in the air gap and the materials of the shield tubes (the outer cylinder)

Fig. 6 shows the gun deformation according to the material changes of a shield tube, where D_{10}^* is the air gap between the gun and the shield tube applied with solar radiation energy and the gun and the shield tube are within the concentric circle. As shown in the figure, the changes in the thermal diffusivity change the gun deformation. The higher the thermal diffusivity, the smaller the gun deformation is M_5, M_6, M_7, which have a higher thermal diffusivity show a relatively small deformation. When FRP (M_1) with a low thermal diffusivity and aluminum (M_5) with a high thermal diffusivity are selected, the flow inside each shield tube according to the air gap changes in the tubes was examined, and the effects of the flow changes on the gun deformation were identified.

Fig. 7 shows the gun deformation according to the changes in the air gap for two materials of different thermal diffusivities. For

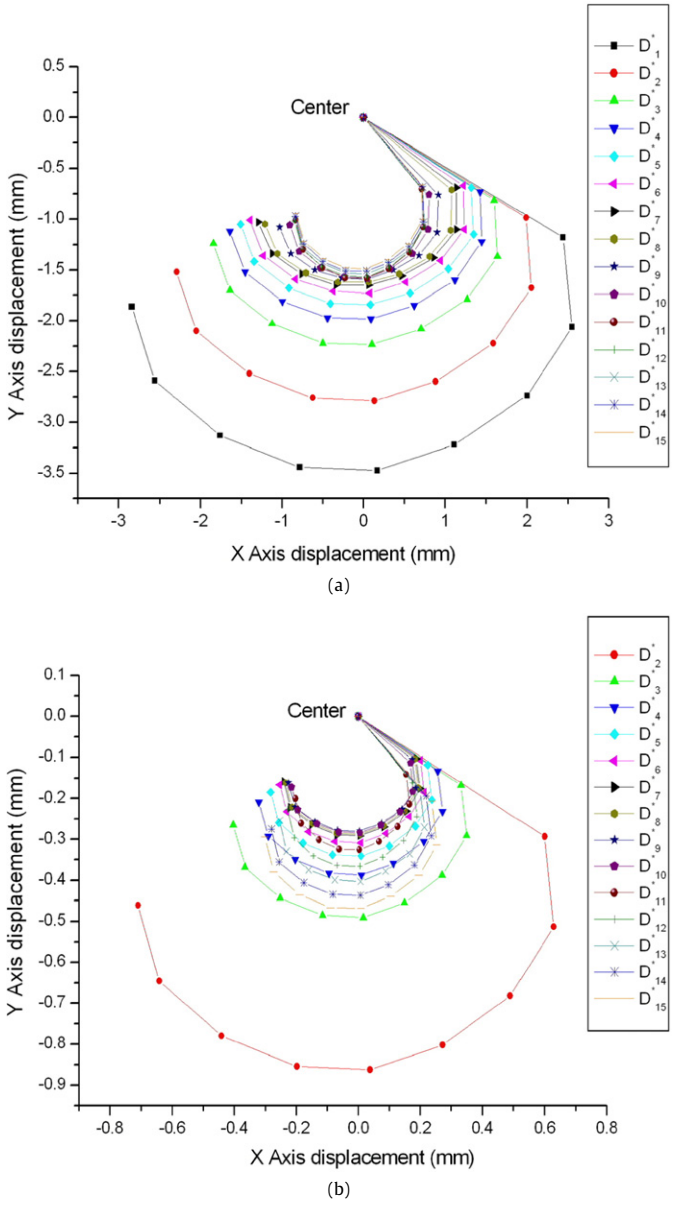

Fig. 7. Gun deformation according to layer of air change and time change. (a) FRP (M_1), (b) aluminium (M_5).

both materials, the gun deformation decreases up to D_{11}^* as the air gap increases;but, particularly, FRP shows a constant gun deformation without decrease after D_{11}^*, and aluminum gives an increase of gun deformation again after D_{11}^*.

Fig. 8 shows the secondary flow intensity depending on the material changes of the shield tube. When the thermal diffusivity is increased, the secondary flow intensity decreases. The secondary flow intensity rapidly decreases from the point of M_4 when the thermal diffusivity starts to increase, and M_5, M_6, M_7 with a higher thermal diffusivity show relatively small secondary flow intensity. Fig. 9 shows the secondary flow intensity according to the air gap changes of some typical materials.

The secondary flow intensity according to the changes of the air gap shows only the changes in the critical points from D_{10}^* to D_{11}^*, as increasing before the critical point while the air gap is increasing from D_2^* to the critical point, and then as decreasing again after the point. With time, a specific amount of energy, that is, the solar radiation energy, transmits heat that leads to natural convection, which is caused by the temperature difference between the inner wall of the shield tube and the outer wall of the gun, and

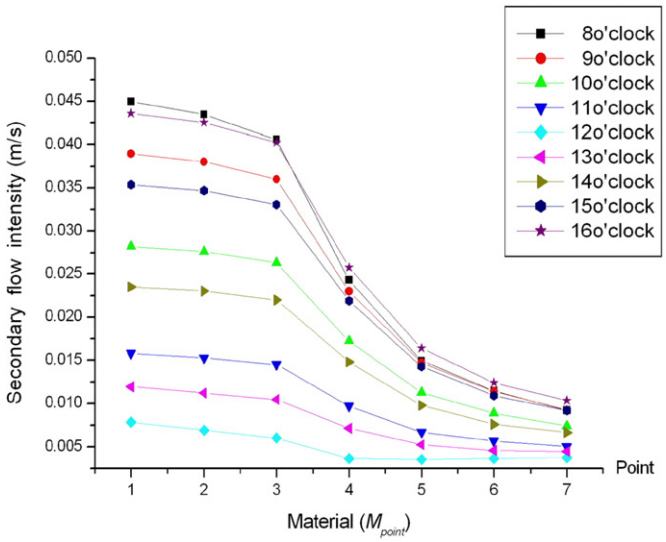

Fig. 8. Secondary flow intensity by shield tube material change.

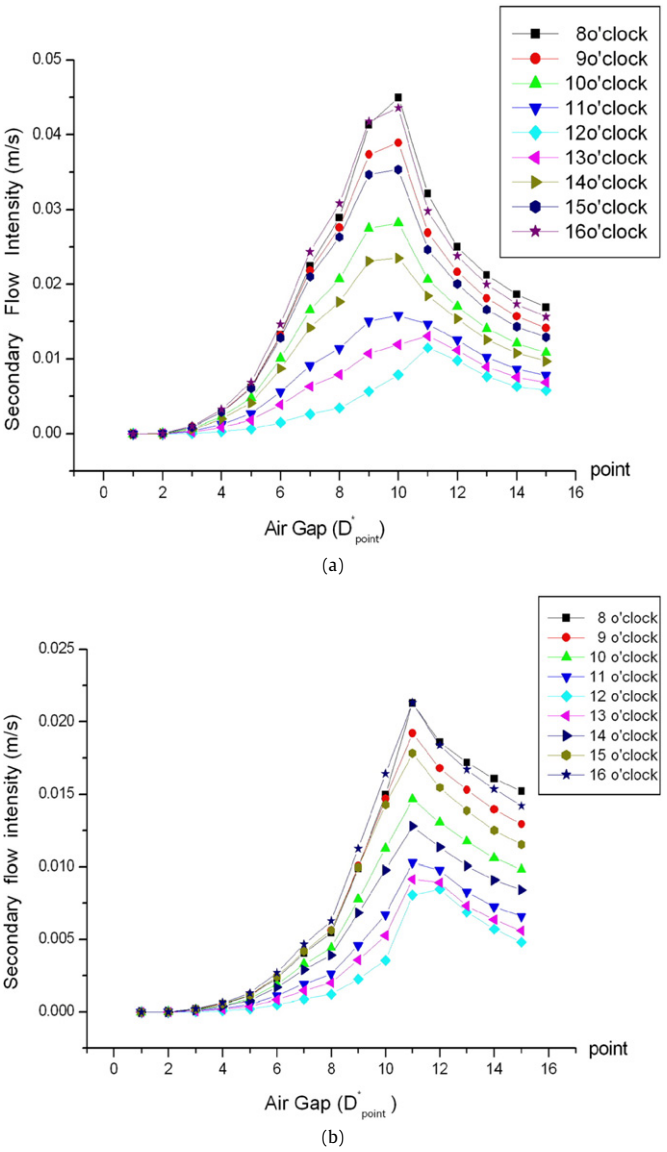

Fig. 9. Secondary flow intensity by air gap change. (a) FRP (M_1), (b) aluminium (M_5).

Table 4
Change of cell number by time change.

Solar hour (o'clock)	8	9	10	11	12	13	14	15	16
M_1	1	1	1	3	4	4	2	1	1
M_2	1	1	1	3	4	4	2	1	1
M_3	1	1	1	3	4	4	1	1	1
M_4	1	1	1	2	4	2	1	1	1
M_5	1	1	1	2	2	2	2	1	1
M_6	1	1	2	2	2	2	2	1	1
M_7	2	2	2	2	2	2	2	2	1

then an active flow circulation occurs as the air gap is expanded; but, when the air layer becomes larger than the critical region, the heat transmission to the gun by the solar radiation energy begins to decrease owing to the expanded air gap. Therefore, the heat sent up to the gun basically decreases. In other words, the areas after the critical point have decreasing secondary flow intensity because there is less energy to cause flow circulation of the expanded air layer. Therefore, a specific source of heat, which was transferred by the solar radiation energy, has a critical region affecting the flow circulation of air inside the shield tube. And, the natural convection flow circulation inside the shield tube is closely related to the gun deformation because the critical point of gun deformation according to the changes in the air layer is the same as that of the secondary flow intensity.

The cause of the differences in the secondary flow intensity in the case of different materials is as follows: in the case of a shield tube with a low thermal diffusivity like FRP, the heat that is transmitted to the directions of its radius and circumference is smaller than that of an aluminum shield tube, so the decreased amount of heat increases the temperature difference between the shield tube and the gun, leading to an increased secondary flow intensity caused by the increase in the temperature difference of the air layer.

Table 4 shows the number of the cells for the air flow according to time and materials. In the case of a shield tube with a low thermal diffusivity, the number of cells of the inner air layer increases as the solar radiation energy approaches to the vertical incidence. While there is at least one or two cells, surrounding a gun without the significant change in the number of the cells (case of a shield tube with a higher thermal diffusivity). The low thermal diffusivity tends to create heat concentration, thereby increasing the temperature difference between the shield tube and the gun. Therefore, the secondary flow intensity increases with the effect of natural convection. Especially, around 12 o'clock, that is the incidence angle of the solar radiation energy, the number of multi-cells is increased. The cells in a local area become activated and cause a stronger flow circulation. If the solar radiation energy is, however, sent tilted, although a shield tube has a low thermal diffusivity, the heat would tend to move to a higher area in the air layer, thereby creating a one-way circulation of the flow, so that the cells circulate without separation, making the temperature of the air layer uniform.

On the contrary, if a shield tube has high thermal diffusivity, the energy would be distributed uniform ly to the direction of its radius and circumference, forming one or two cells without multi-cells uniform around 12 o'clock when the heat has a strong tendency of being divided into upper and lower parts. Those cells start to cover largely a gun, flow circulating around the gun, to make gun surface temperature uniform. Consequently, the cells have a great influence on the decrease of the gun deformation.

As a more detailed description on the phenomena described above, the following is the findings on the distribution of the isothermal lines and streamlines of air for some typical materials.

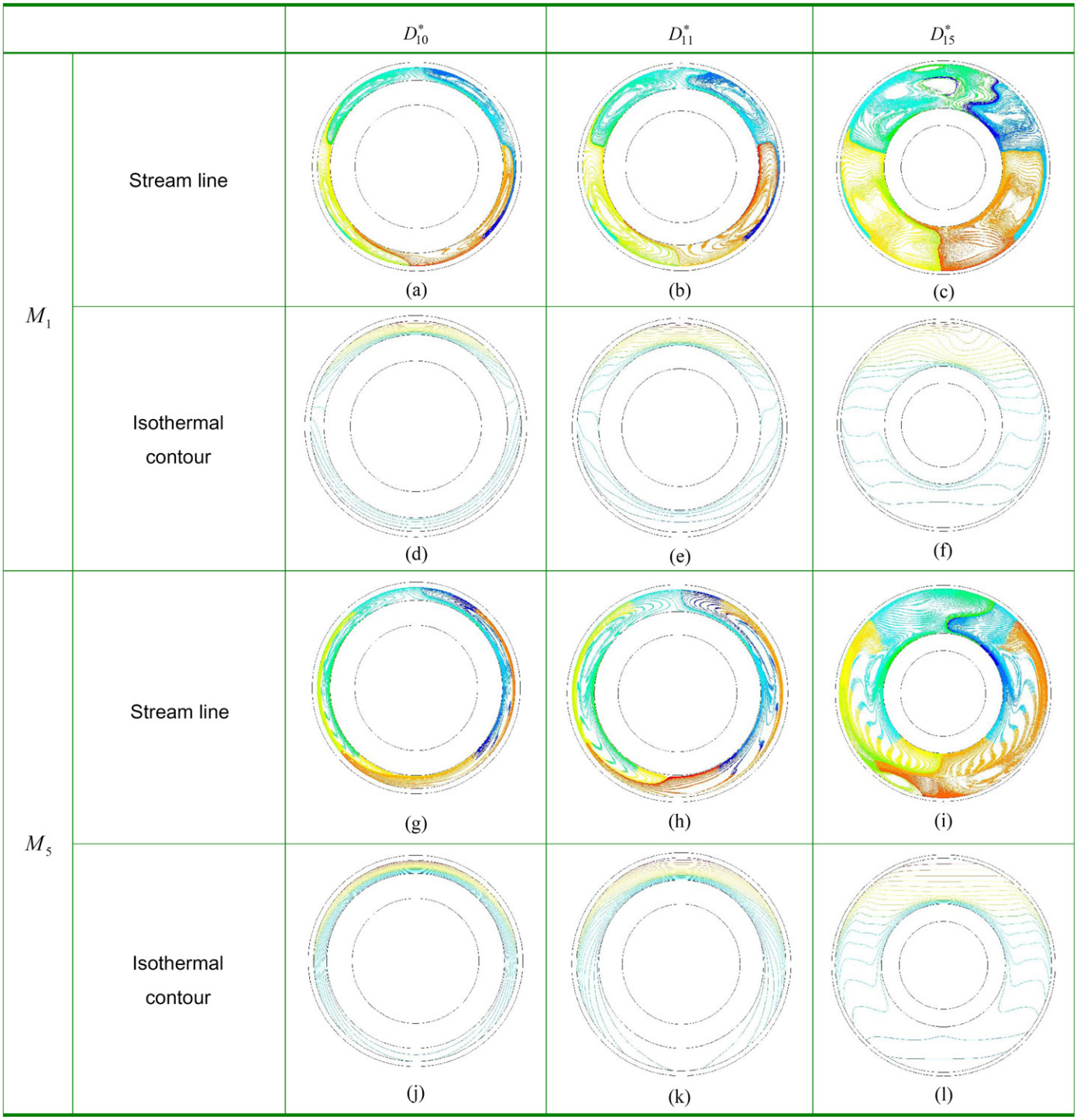

Fig. 10. Streamlines and isothermal lines by air gap change (12 o'clock).

Fig. 10 shows the isothermal lines and streamlines of air according to the changes in the air gap with different thermal diffusivities, under the time condition of 12 o'clock.

M_1 with low thermal diffusivity has relatively small cells activated locally, while M_5 with high thermal diffusivity has large cells activated over a broad region in the direction of the circumference. The features of the air flow according to material changes become more apparent with consideration of the distribution of isothermal lines. M_1, which has low thermal diffusivity, has isothermal lines that are divided clearly into the upper and lower parts, whereas M_5, which has high thermal diffusivity, shows lines covering the gun in a concentric circle. That is, the kinds of M_1 with low thermal diffusivity make the heat transmitted to a shield tube by the solar radiation energy accumulate, not transmitting the heat fast to the directions of its radius and circumference. Therefore, the layer of temperature is divided from the incidence point of the energy into the upper and lower parts, so the air layer comes forms cells as it is relatively divided into upper and lower parts to cause flow circulation. That phenomenon increases the temperature difference over the shield tube and the Rayleigh number and promotes the natural convection, thereby raising the secondary flow intensity. On the contrary, the kinds of M_5 with high thermal diffusivity have

isothermal lines covering the gun in a concentric circle. Grighll and Hauf [5] stated that in this type of situation, isotherms in a narrow horizontal cylinder space have a shape of a concentric circle and there is heat transmission in the concentric circle shape as the pseudo-conductive phenomenon, and the natural convection of the fluid in a cylinder is similar as the thermal conduction of a solid through the movement of electrons. This means that there is pseudo-conduction in the materials with high thermal diffusivity. The solar radiation energy on a shield tube is distributed uniformly to the direction of the circumference, not accumulated at a specific point because of the dispersion of heat caused by higher thermal diffusivity, and this uniform distribution decreases the temperature difference between the inner and outer walls of the air layer. Then, the layer strongly tends to form a larger single cell, instead of making an activated natural convection. The heat sent through such a process is transmitted to the gun, making the entire temperature uniform. This conduction weakens the natural convection in an air layer and increases the secondary flow intensity. But, the strong heat transfer through the air layer to the gun makes the gun temperature uniform and decreases its deformation. In brief, a shield tube of material with high thermal diffusivity the inner air layer has a relatively low temperature difference, inhibiting natural convection. Therefore, its air layer is close to the stationary state, which becomes similar as the conduction of solid, that is, pseudo-conductive phenomenon. For this reason, M_5 gives a smaller deformation of the gun than that of M_1 despite of its lesser natural convection flow by the smaller secondary flow intensity, compared to M_1.

The following is about the changes in the streamlines and isotherms according to the air gap changes. Based on the finding that the secondary flow intensity decreases in the air gap over D_{10}^* to D_{11}^* uniform when the air gap is increasing, it can be found out that the flow circulation does not make the gun temperature uniform. The areas after D_{10}^* to D_{11}^* have such an expanded air gap that there is relatively little heat transmitted to the gun from the shield tube by the solar radiation energy. This is apparent when checking the obvious change in the temperature difference when the air gap is expanded from D_{10}^* to D_{11}^*: the isothermal lines in the air layer, which spread to the direction of the circumference, become horizontal gradually after the air gap D_{11}^*, and these horizontal lines are more obvious at D_{15}^*. There is a stationary state of temperature after D_{11}^*, caused by the decreased secondary flow intensity. Gun deformation shows a different tendency according to the different material for the shield tube in the critical region where D_{10}^* to D_{11}^*. In the case of FRP (low thermal diffusivity), the expanded air gap decreases the thermal transmission to the gun, so the gun deformation is reduced. But, the aluminum shield tube increases the deformation again after the critical region D_{11}^*. This means that both the materials with different thermal diffusivities have a critical region from D_{10}^* to D_{11}^* as an air gap that makes the gun temperature uniform through the flow circulation caused by the natural convection by the transmitted heat: the deformation of the gun with the FRP material does not have significant relations with the air gap and the secondary flow intensity; the aluminum material shows significant relations with them after the critical region of the air layer. Therefore, in the case of a shield tube with high thermal diffusivity, gun deformation is more influenced by the pseudo-conductive phenomenon than the flow circulation of the natural convection in making the gun temperature uniform. The materials of shield tubes with relatively higher thermal diffusivity inhibited the natural convection. Taken together, a double cylinder heated uniformly has its air gap in organic relations with the thermal diffusivity of its materials, and the thermal diffusivity and the critical region of the layer of air are the significant factors affecting the deformation of a gun.

Table 5
Average Nusselt number by air gap change (outer cylinder (M_1)).

Cylinder diameter point	Air gap	8 o'clock	10 o'clock	12 o'clock	14 o'clock	16 o'clock
d_2	D_1^*	0.3359	0.3362	0.3364	0.3316	0.3343
	D_{10}^*	0.4789	0.3966	0.5068	0.3752	0.4234
	D_{15}^*	0.8266	0.6055	0.4430	0.5133	0.9180
D_1	D_1^*	0.3382	0.3378	0.3376	0.3487	0.3409
	D_{10}^*	0.3484	0.3560	0.6393	0.4771	0.3878
	D_{15}^*	0.7162	0.5704	0.5912	0.4902	0.4236

3.3. Variation of Nusselt numbers on the cylinder wall surfaces

Local heat transfer coefficient of cylinder surface is defined as

$$h_\theta = \frac{q_\theta}{T_{s\theta} - T_{b\theta}} \tag{16}$$

where q_θ is the local heat flux at θ degree; $T_{s\theta}$ is the local surface temperature; $T_{b\theta}$ is the local bulk mean air temperature at θ degree. q_θ and $T_{b\theta}$ are given by

$$q_\theta = -k_{\text{air}}\left(\frac{\partial T}{\partial r}\right) \tag{17}$$

$$T_{b\theta} = \frac{1}{L}\int_{r=r_2}^{r=R_1} T_{br}\, dr \tag{18}$$

where L is $R_1 - r_2$ and k_{air} is the thermal conductivity of air. T_{br} is local air temperature.

The local Nusselt number (Nu_θ) is defined as:

$$Nu_\theta = \frac{h_\theta L}{k_{\text{air}}} \tag{19}$$

The average values of Nusselt number ($\overline{Nu_\theta}$) can be calculated based on the average heat transfer coefficient as follows:

$$\overline{h_\theta} = \frac{1}{2\pi}\int_0^{2\pi} h_\theta\, d\theta \tag{20}$$

$$\overline{Nu_\theta} = \frac{\overline{h_\theta} L}{k_{\text{air}}} \tag{21}$$

Table 5 shows the variation of average Nusselt number with respect to air layer thickness.

According to the increase in air layer thickness between the double cylinders, the natural convection is activated so that it may increase the average Nusselt numbers of the surfaces. In the case of air gap thickness, D_{15}^* at 12 o'clock, average Nusselt number decreases again. At 12 o'clock, solar energy irradiated vertically on the shield tube produces symmetric circulations of natural convection in the air layer so that it may suppress the natural convection.

Fig. 11 shows the local Nusselt number of cylinder wall with respect to the air layer thickness. Peaks of local Nusselt numbers are shown at 30°–60° and 210°–240° circumferential area of outer cylinder. These regions represent the boundary layer between upper area of hot temperature and lower area of cold temperature of outer cylinder irradiated by solar energy. Small temperature difference between boundary layers leads to the increase in local Nusselt number. Opposite side of outer cylinder wall on which solar energy is irradiated, thermal conduction effect becomes more important. We can see that local Nusselt numbers increase in accordance with the increase in air layer thickness. This is caused by the activation of natural convection with the increase in air gap thickness. As shown in the case of 12 o'clock at which solar energy is irradiated vertically, after the critical area of air layer thickness, promotion of natural convection decreases again.

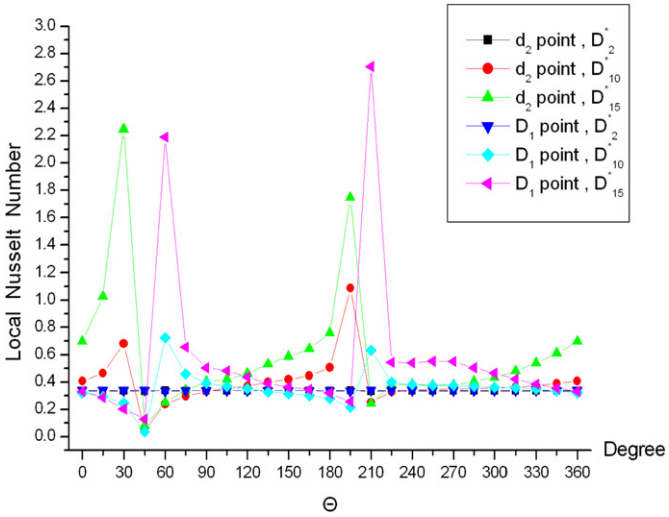

Fig. 11. Local Nusselt number by layer of air change (10 o'clock).

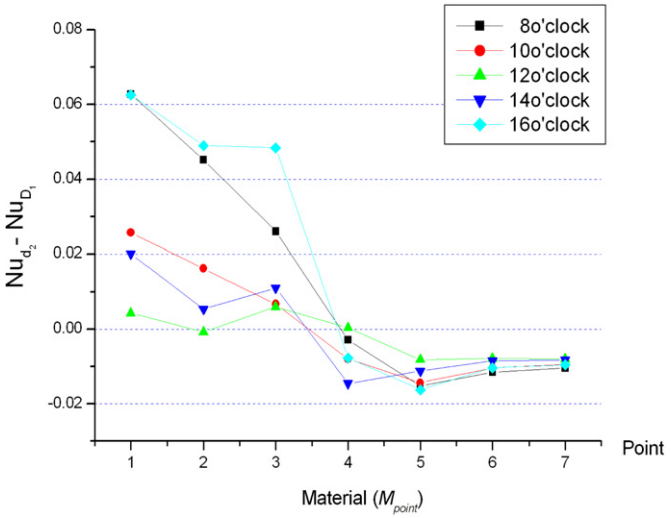

Fig. 13. Average Nusselt number difference between inner (Nu_{d_2}) and outer cylinders (Nu_{D_1}) with respect to shield tube materials.

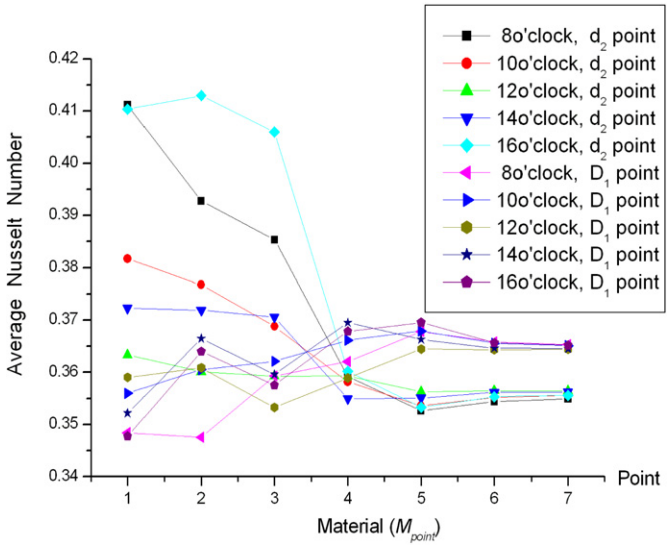

Fig. 12. Variation of average Nusselt number of with respect to shield tube materials.

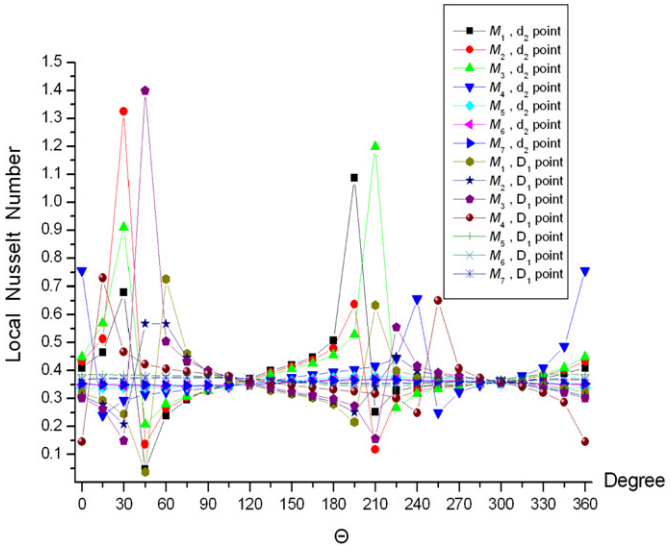

Fig. 14. Variation of local Nusselt number inner wall surface of outer cylinder with respect to material thermal conductivities (10 o'clock).

Fig. 12 shows the variation of average Nusselt number of cylinder wall with respect to the shield tube materials in the case of air gap thickness, D_{10}^*. Time variation of Nusselt Number difference ($Nu_{d_2} - Nu_{D_1}$) between inner and outer cylinders in the case of air gap thickness, D_{10}^* is shown in Fig. 13. In the cases of low thermal conductivity of outer materials, M_1–M_3, average Nusselt number of inner cylinder is smaller than average Nusselt number of outer cylinder. On the other hand, in the cases of high thermal conductivity of outer cylinder materials, M_5–M_6, average Nusselt number of inner cylinder is larger than average Nusselt number of outer cylinder. That is, outer cylinder materials with high thermal conductivity promote thermal conduction phenomena in the inner cylinder wall and make air layer temperature between the cylinders uniformly so that it reduce the thermal deformation of inner cylinder.

Fig. 14 shows variation of local Nusselt number of shield tube surface with respect to material properties for at 10 o'clock. In this figure, higher the thermal conductivity of outer cylinder material, local Nusselt number variations of outer and inner cylinder surfaces decrease in circumferential direction. This phenomenon can be explained as follows. Balance of conduction heat transfer and natural convection in the gap between inner and outer cylinders may exert an influence on the uniformity of air layer temperature. This mechanism makes the air layer temperature in the gap between cylinders uniformly so that it plays an important part in reducing the thermal deformation of gun.

4. Conclusions

1. In the case of an outer cylinder (a shield tube) with a higher thermal diffusivity, it is rather the heat transmitted to the direction of its radius and circumference into an inner cylinder (a gun) by the pseudo-conductive phenomenon in the air layer, than the flow circulation of the natural convection, that makes uniform the temperature of the inner cylinder, thereby decreasing the deformation of the gun.
2. If an outer cylinder has high thermal diffusivity, there is little temperature difference in the outer cylinder, showing a state of uniform heating and inhibited natural convection, so the air layer gets closer to a stationary state, which leads to the pseudo-conductive phenomenon similar to conduction in a solid. Consequently, the materials of the outer cylinders with high thermal diffusivity inhibited the natural convection.

3. In the areas before the critical region of air, that is, D^*_{10} to D^*_{11} $(1.149 \leqslant D^*_{\text{point}} = (D_1/d_2) \leqslant 1.268)$, the secondary flow intensity increased as the air gap increased, regardless of the material changes of the outer cylinder. The gun deformation, consequently, decreased by the flow circulation of the natural convection to make the air layer temperature uniform. But, in the areas after the critical region, the secondary flow intensity decreased as the air gap increased, regardless of the material changes of the outer cylinder. The natural convection flow in the air layer became inhibited and the gun deformation showed a different tendency of being increased again or being constant according to the thermal diffusivities of different materials. The gun deformation is thus more affected by the flow circulation of the natural convection before the critical region of the air layer and more influenced by the thermal diffusivity of materials after the critical region. Consequently, the air gap and the thermal diffusivity of materials have close relations to each other and are significant factors affecting the deformation of the inner cylinder.
4. Higher the thermal conductivity of shield tube, variations of local Nusselt numbers of outer and inner cylinder surfaces decrease due to the activation of natural convection and the balance of conduction heat transfer and natural convection in the gap between inner and outer cylinders.

References

[1] W. Beckmann, Die Warmeubertragung in Zylindrischen Gasschichten bei naturlicher Konvektion, Forschung, im ingeniuerwesen 2 (1931) 165–178.
[2] E.R.G. Eckert, E.E. Soehngen, Studies on heat transfer in laminar free convection with the Mach–Zehnder interferometer, Wright–Patterson AFB Tech, ATI-44580, 1948, Rept. 5747.
[3] U. Grigull, W. Hauf, Natural convection in horizontal cylindrical annuli, in: Third Int. Heat Transfer Conf., vol. 2, 1966, pp. 182–195.
[4] T.H. Kuehn, R.J. Goldstein, An experimental study of natural convection heat transfer in concentric and eccentric horizontal cylindrical annuli, J. Heat Transfer, ASME 100 (1978) 635–640.
[5] U. Grigull, W. Hauf, Natural convection in horizontal cylindrical annuli, in: Third Int. Heat Transfer Conf., vol. 2, 1966, pp. 182–195.
[6] L. Crawford, R. Lemlich, Natural convection in horizontal concentric cylindrical annuli, I & EC Fund. 1 (1962) 260–264.
[7] U. Grighll, W. Hauf, Natural convection in horizontal cylindrical annuli, in: Proc. of 3rd International Heat Transfer Conference, vol. 2, 1966, pp. 182–195.
[8] L.R. Mack, E.H. Bishop, Natural convection between horizontal concentric cylinders for low Rayleigh numbers, Quarterly Journal of Mechanics and Applied Mathematics 21 (1968) 223–241.
[9] T.H. Kuehn, R.J. Goldstein, An experimental and theoretical study of natural convection in the annulus between horizontal concentric cylinders, J. Fluid Mech. 74 (1976) 695–719.
[10] Y.F. Rao, Y. Miki, K. Fukuda, Y. Takata, S. Hasegawa, Flow patterns of natural convection in horizontal cylindrical annuli, Int. J. Heat Mass Transfer 28 (1985) 705–714.
[11] A. Castrejon, D.B. Spalding, An experimental and theoretical study of transient free-convection between horizontal concentric cylinders, Int. J. Heat Mass Transfer 31 (1988).
[12] F.A. Hamad, M.K. Khan, Natural convection heat transfer in horizontal and inclined annuli of different diameter ratios, Energy Covers. Mgmt 39 (1988) 797–807.
[13] J.S. Yoo, Dual steady solutions in natural convection between horizontal concentric cylinders, Int. J. Heat Fluid Flow 17 (1996) 587–593.
[14] J.S. Yoo, Natural convection in a narrow horizontal cylindrical annulus, Int. J. Heat Mass Transfer 41 (1998) 3055–3073.
[15] J.S. Yoo, Transition and multiplicity of flows in natural convection in a narrow horizontal cylindrical annulus: $Pr = 0.4$, Int. J. Heat Mass Transfer 42 (1999) 709–722.
[16] J.S. Yoo, Prandtl number effect on bifurcation and dual solutions in natural convection in a horizontal annulus, Int. J. Heat Mass Transfer 42 (1999) 3279–3290.
[17] Horng Wen Wu, Wen Ching Tsai, Huann-Ming Chou, Transient natural convection heat transfer of fluids with variable viscosity between concentric and vertically eccentric spheres, Heat and Mass Transfer 47 (2004) 1685–1700.
[18] J. Mizushima, S. Hayashi, T. Adachi, Transitions of natural convection in a horizontal annulus, Int. J. Heat Mass Transfer 44 (2001) 1249–1257.
[19] F. Shahraki, Modeling of buoyancy-driven flow and heat transfer for air in a horizontal annulus; effects of vertical eccentricity and temperature-dependent properties, Numer. Heat Transfer Part A 42 (2002) 603–621.
[20] G. Petrone, E. Chenier, G. Lauriat, Stability of free convection in air filled horizontal annuli: influence of the radius ratio, Int. J. Heat Mass Transfer 47 (2004) 3889–3907.
[21] N.A. Roschina, A.V. Uvarov, A.I. Osipov, Natural convection in an annulus between coaxial horizontal cylinders with internal heat generation, Int. J. Heat Mass Transfer 48 (2005) 4518–4525.
[22] A.M. Al-Amiri, K.M. Khanafer, Numerical simulation of double-diffusive mixed convection within a rotating horizontal annulus, Int. J. Thermal Sci. 45 (2006) 567–578.
[23] J.C. Leong, F.C. Lai, Natural convection in a concentric annulus with a porous sleeve, Int. J. Heat Mass Transfer 49 (2006) 3016–3027.
[24] T. Adachi, S. Imai, Three-dimensional linear stability natural convection in horizontal concentric annuli, Int. J. Heat Mass Transfer 50 (2007) 1388–1396.
[25] Fluent Incorporated, Fluent 6.1.22, User's Guide, 2003.
[26] ASHRAE, Handbook of Fundamentals 1979, American Society of Heating, Refrigeration, and Air-Conditioning Engineers, New York, 1979.
[27] ANSYS Incorporated, ANSYS 10.0.